Scaled electron ionization cross sections in the Born approximation for atoms with $55 \leq Z \leq 102$

Eugene J. McGuire
Sandia Laboratories, Albuquerque, New Mexico 87115
(Received 12 March 1979)

Using the generalized oscillator-strength formulation of the Born approximation, the author calculated electron ionization cross sections for all significant subshells of every fourth atom with $58 \leq Z \leq 102$, and for Hg. The calculations used approximate Herman-Skillman wave functions and eigenvalues. The cross sections were put in scaled form, depending essentially on ionization energy only. The scaled cross sections were used with experimental energies to calculate the cross sections for Cs, Cs^+, Ba, Ba^+, Au, Hg, Tl, Tl^+, and Pb. The cross sections so calculated were in good agreement with the measurements. Both inner-shell ionization and excitation followed by autoionization were prominent contributors to the cross section. The scaling procedure was used to calculate the electron ionization cross section of the noble-gas metastable levels, and there is excellent agreement with measured valves for Ne and A. The scaling procedure was used to calculate cross sections for the sequential ionization Ni^{+1}–Ni^{+14} and Au^{+3}–Au^{+14}, which were compared with cross sections obtained from the semiempirical expression of Lotz. Good agreement was found for the Ni ions, but there was poor agreement for the Au ions. Lotz's expression is a factor of 3 smaller than our scaled cross section for the $4d$, $4f$, and $5d$ subshells. It is suggested that the absence of measurements on these subshells precluded correct parametrization in the semiempirical expression of Lotz.

I. INTRODUCTION

Accurate electron-ionization cross sections for high-Z elements are required in modeling energy deposition in relativistic electron beam fusion pellets, in modeling the interaction of focused high-intensity laser beams with high-Z targets, and in modeling the effects of high-Z impurities in magnetic confinement fusion systems. At present the semiempirical electron-ionization cross section of Lotz[1] is widely used in such models. Lotz's expression is parametrized with constants chosen to give the best fit to a variety of experimental measurements, principally on low-Z ($Z \leq 54$) elements. Consequently, it cannot critically evaluate contradictory measurements; Lotz's expression is not properly parametrized for $4f$ electrons, since there are no measurements on electron-ionization cross sections sensitive to σ_{4f} [e.g., no measurements on Y ($Z=70$)]; and it uses a limited data base of high-Z measurements.

Recently I presented calculations[2] of electron-ionization cross sections for elements with $19 \leq Z \leq 54$ using the generalized oscillator strength (GOS) formulation of the Born Approximation (BA). The calculated total electron-ionization cross sections were in excellent agreement with measurements on Kr and Xe above 400 eV, in agreement with one of two sets of contradictory measurements in Mg, and in agreement with one of three sets of contradictory measurements on Cu.

In this sense the BA calculations provide a means of critically evaluating contradictory measurements. These critical evaluations in the $19 \leq Z \leq 54$ region will be useful in examining disagreements between the calculations and experiment for $Z > 54$, when only a single set of measurements is available. In addition it was shown that electron-ionization cross sections could be scaled via $\sigma_{nl}(E_I^{nl})^{\alpha(nl)} = f_{nl}(\epsilon/E_I^{nl})$, where σ_{nl} is the electron-ionization cross section for the nl subshell, E_I^{nl} is the ionization energy, f_{nl} is a function of the ratio of incident electron energy to ionization energy, and $\alpha(nl)$ is a parameter which depends on E_I^{nl}, but for sufficiently large E_I^{nl}, $\alpha = 2$ (classical scaling). The scaling property suggests that electron-ionization cross sections for almost all atoms in all stages of ionization can be represented by 19 scaled subshell cross sections, and that the scaling parameters $\alpha(nl)$ and f_{nl} can be obtained from calculation on selected subshells of selected atoms. In Ref. 3 the scaled cross sections obtained from neutral atoms were applied to the calculation of electron-ion-ionization cross sections. For some systems (e.g., Na^{+1}, Mg^{+2}) the agreement with measured cross sections was excellent, while for others (e.g., O^{+1}, O^{+2}) the calculated cross section was 40% lower than the measurements. Currently, the hypothesis that this disagreement is a configuration interaction effect between $(2s)^2(2p)^n$ and $(2s)^0(2p)^{n+2}$ is being investigated.

In this paper I report cross-section calculations for selected high-Z neutral atoms. The calculations were for all interesting (i.e., nonclassical) subshells of every fourth element between $58 \leq Z \leq 102$, and for Hg ($Z=80$). The assumptions in the calculations are discussed in Ref. 2. Expressions for the one-electron GOS for s, p, and d electrons are given in Eq. (2) of Ref. 2. For f electrons the one-electron GOS is given by

$$\frac{k^2}{\Delta E}\frac{df_{n3}}{d\epsilon}=\frac{5}{2}\frac{(l'-2)(l'-1)(l')}{(2l'-1)(2l'-3)}R_{l,l',l'-3}$$
$$+\frac{3}{2}\frac{(l'-1)(l')(l'+1)}{(2l'+3)(2l'-3)}R_{l,l',l'-1}$$
$$+\frac{5(l'+3)(l'+2)(l'+1)}{2(2l'+5)(2l'+3)}R_{l,l',l'+3},$$
$$+\frac{3}{2}\frac{l'(l'+1)(l'+2)}{(2l'+5)(2l'-1)}R_{l,l',l'+1},$$

where

$$R_{l,l't}=\left|\int_0^\infty j_t(kr)\,\phi_{n3}(r)\,\phi_{\epsilon l'}(r)\,dr\right|^2,$$

$j_t(z)$ is a spherical Bessel function, and ϕ_{nl} are atomic orbitals.

Since the calculations were done for every fourth element the results are presented as scaled cross section in Sec. II. In Sec. III the scaled cross sections are used for calculations on all high-Z neutral atoms and ions for which measurements are available. In Sec. IV the scaled cross sections are used to calculate cross sections for electron ionization of the $(np)^5[(n+1)s]$ configurations of the noble gases. The results are compared with recent calculations of Ton-That and Flannery.[4]

In Sec. V the scaled cross sections are used to calculate cross sections for sequential ionizations of Ni and Au to examine the effect of the $4f$ shell. Similar cross sections via the Lotz formula are included. Conclusions are presented in Sec. VI. The calculations for elements with $Z>54$ showed that the $3s$, $3p$, and $3d$ subshell cross sections had reached the classical scaling region at Xe. Thus, the prescription in Sec. III of Ref. 3 can be used to extend the scaled $n=3$ subshell cross sections to the classical scaling region.

II. SCALED CROSS SECTIONS

The parameter $\alpha(nl)$ in the scaled subshell cross sections is found by plotting $\sigma_{nl}^{\max}(E_I^{nl})^2$. For classical scaling $\alpha(nl)=2$ and the plot is a horizontal line. In Fig. 1 such a plot is shown for $4s$ and $4d$ electrons. Throughout, the calculations are normalized to filled subshells. In both cases there are four regions of different $\alpha(nl)$. In each region a representative element is chosen from which $f_{nl}(\eta)$ is determined, with $\eta=\epsilon/E_I^{nl}$. The function $f_{nl}(\eta)$ is different in each region and $f_{nl}(\eta)/f_{nl}(\eta)$ (max), a normalized shape function, differs in each region, particularly at high η. This presents a small problem for $4f$ electrons. In Fig. 2 $\sigma_{nl}(E_I^{nl})^2$ vs E_I^{nl} is shown for $4p$ and $4f$ electrons. The remarkable feature is the monotonic rise in $\sigma_{4f}(E_I^{4f})^2$. Even though there are 14 $4f$ electrons

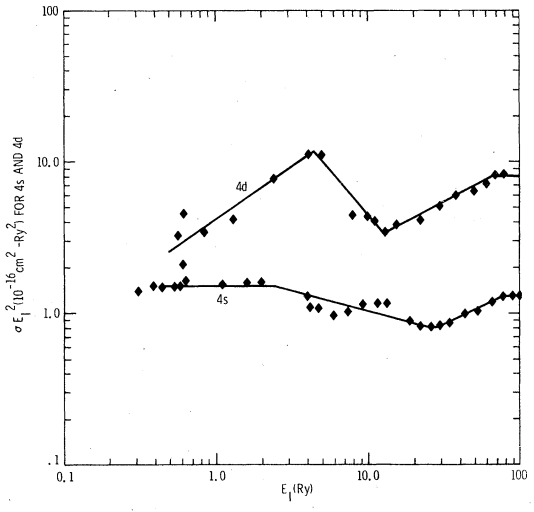

FIG. 1. Calculated $\sigma_{\max}(E_I)^2$ for $4s$ and $4d$ subshells.

and 2 ns electrons, for $E_I^{4f}\leq 3.0$ Ry, the $4f$ peak cross section is smaller than or comparable to the ns cross sections for equal E_I. Further, the $4f$ calculations in Fig. 2 can be fitted by a single $\alpha(4f)$ value for $0.3<E_I^{4f}<40$ Ry. There is no division into regions in each of which there is a different $f_{4f}(\eta)$. In Fig. 3 normalized $4f$ cross sections as a function of η are plotted for $Z=58$, 78, 90, and 102. Representative points of normalized $4f$ cross sections for $Z=62$, 66, and 70 are seen to lie on the curve for $Z=58$; representative points for $Z=74$ and 82 are within 20% of the $Z=78$ curve; while points for $Z=86$ are with 20% of the $Z=90$ curve. This enables one to divide the monotonic

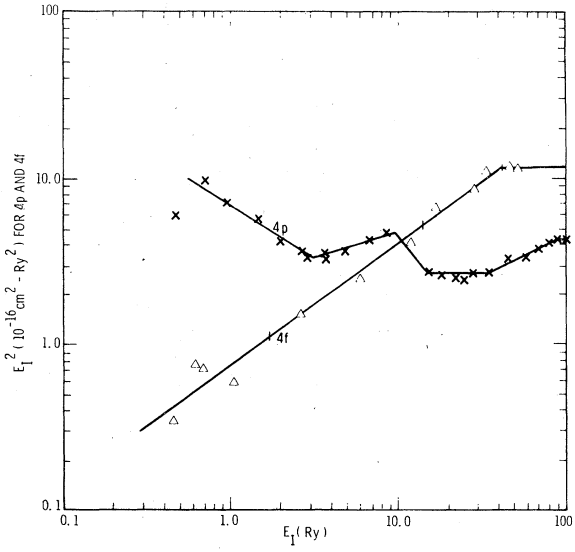

FIG. 2. Calculated $\sigma_{\max}(E_I)^2$ for $4p$ and $4f$ subshells.

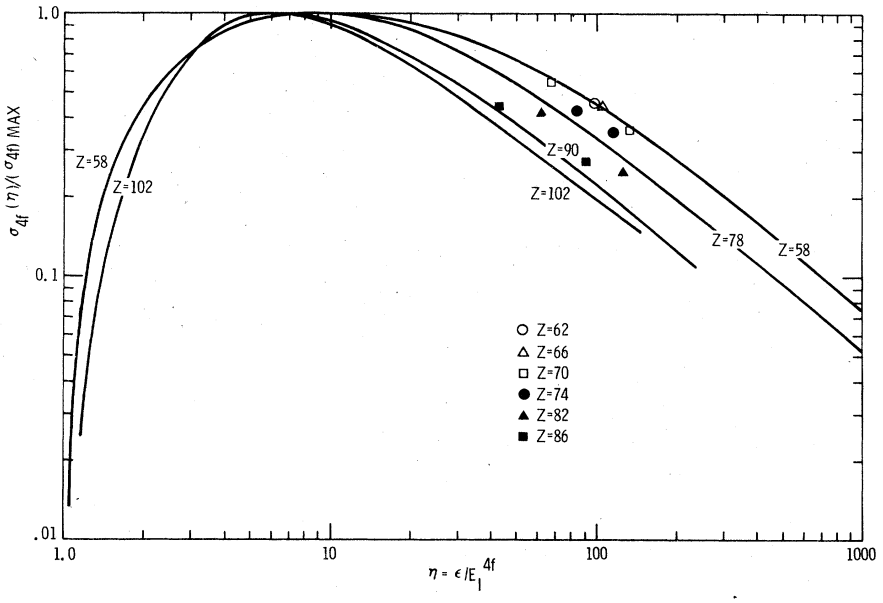

FIG. 3. Normalized $[\sigma(\epsilon)/\sigma(\epsilon)$ max] $4f$ subshell cross sections for $Z = 58$, 78, 90, and 102, to show shape variation. The circles, triangles, and squares are points of the normalized cross section at $Z = 62$, 66, 74, 82, and 86.

TABLE I. Parameters for the scaled $4s$ and $4p$ electron-ionization cross sections; $\sigma_{nl}(\epsilon)(E_I^{nl})^{\alpha} = f_i(\epsilon/E_I^{nl})$, with f in units of 10^{-16} cm^2 Ry$^{\alpha}$. The subscripts a–f refer to the following values for α and E_I^{nl}.

$4s$	$4p$
a: $0.3 \leq E_I \leq 2.5$, $\alpha = 2.00$	a: $0.6 \leq E_I \leq 3.0$, $\alpha = 2.62$
b: $2.5 \leq E_I \leq 27$, $\alpha = 2.26$	b: $3.0 \leq E_I \leq 9.5$, $\alpha = 1.68$
c: $27 \leq E_I \leq 80$, $\alpha = 1.52$	c: $9.5 \leq E_I \leq 15$, $\alpha = 3.29$
d: $80 \leq E_I$, $\alpha = 2.00$	d: $15 \leq E_I \leq 35$, $\alpha = 2.00$
	e: $35 \leq E_I \leq 90$, $\alpha = 1.48$
	f: $90 \leq E_I$, $\alpha = 2.00$

η	f_a	f_b	f_c	f_d	η	f_a	f_b	f_c	f_d	f_e	f_f
1.25	0.50	0.52	0.075	0.25	1.25	1.10	0.27	18.0	0.52	0.050	1.10
1.50	0.84	0.86	0.160	0.53	1.50	2.30	0.69	40.0	1.08	0.120	1.90
1.75	1.13	1.12	0.240	0.76	1.75	3.70	1.20	56.0	1.50	0.200	2.60
2.0	1.32	1.30	0.305	0.92	2.0	4.65	1.70	65.0	1.82	0.275	3.15
2.5	1.50	1.57	0.400	1.12	2.5	6.00	2.35	77.0	2.25	0.360	3.95
3.0	1.52	1.71	0.460	1.22	3.0	6.70	2.30	83.0	2.55	0.390	4.22
3.5	1.50	1.80	0.510	1.27	3.5	6.80	2.28	86.0	2.67	0.402	4.35
4.0	1.44	1.83	0.530	1.29	4.0	6.75	2.20	89.0	2.74	0.403	4.38
5.0	1.32	1.75	0.540	1.25	5.0	6.45	2.03	86.0	2.70	0.400	4.25
6.0	1.20	1.68	0.520	1.18	6.0	6.00	1.85	82.0	2.60	0.380	3.90
7.0	1.10	1.60	0.490	1.10	7.0	5.50	1.70	78.0	2.45	0.360	3.60
8.0	0.98	1.50	0.460	1.00	8.0	5.15	1.60	74.0	2.30	0.335	3.32
10.0	0.82	1.35	0.410	0.88	10.0	4.40	1.35	66.0	2.00	0.290	2.88
15	0.58	1.04	0.315	0.68	15	3.30	1.00	50.0	1.53	0.220	2.17
20	0.45	0.84	0.255	0.56	20	2.60	0.80	40.0	1.24	0.178	1.75
25	0.36	0.72	0.215	0.46	25	2.15	0.67	34.0	1.05	0.150	1.48
30	0.30	0.62	0.188	0.41	30	1.85	0.57	29.0	0.90	0.130	1.29
40	0.225	0.48	0.150	0.325	40	1.45	0.45	23.0	0.70	0.103	1.00
50	0.185	0.41	0.125	0.270	50	1.18	0.37	19.0	0.58	0.086	0.84
60	0.155	0.35	0.107	0.230	60	1.00	0.31	16.2	0.49	0.074	0.71
80	0.115	0.27	0.083	0.180	80	0.77	0.24	12.7	0.38	0.058	0.55
100	0.093	0.22	0.068	0.147	100	0.62	0.19	10.4	0.30	0.047	0.44

$4f$ curve into four regions. Scaled cross sections for the $4l$ subshells are shown in Tables I and II.

In Figs. 4 and 5, $\sigma_{5l}^{\max}(E_I^{5l})^2$ for the $5s$ and $5d$, and $5p$ and $5f$ subshells, respectively, are shown. There are a limited number of points for $5d$ and $5f$ subshells. Within the range of the calculations, scaled cross sections for the $5l$ subshells were calculated and are shown in Tables III and IV. Table V lists the scaled cross sections for the $6s$ and $6p$ subshells. In Fig. 6 $\sigma_{nl}(E_I^{nl})$ is shown for $6d$ and $7s$ electrons. The limited number of elements and the small spread in ionization energy restrict the scaling to the narrow range shown in Table VI.

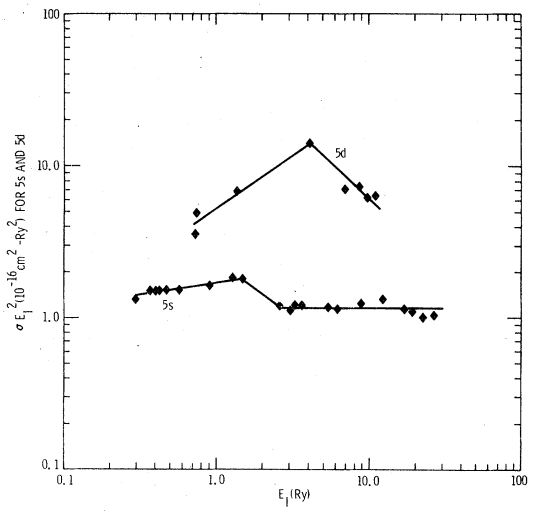

FIG. 4. Calculated $\sigma_{\max}(E_I)^2$ for $5s$ and $5d$ subshells.

III. COMPARISON WITH EXPERIMENT

In using the scaled cross sections to compare the calculations with experiment, the ionization thresholds used are taken from Moore's tables[5]

TABLE II. Parameters for the scaled $4d$ and $4f$ electron-ionization cross sections; $\sigma_{nl}(\epsilon)(E_I^{nl})^\alpha = f_i(\epsilon/E_I^{nl})$, with f in units of 10^{-16} cm^2 Ry$^\alpha$. The subscripts a–d refer to the following values for α and E_I^{nl}.

$4d$					$4f$				
a: $0.5 \le E_I \le 4.4$, $\alpha = 1.30$					a: $0.4 \le E_I \le 1.7$, $\alpha = 1.26$				
b: $4.4 \le E_I \le 13$, $\alpha = 3.16$					b: $1.7 \le E_I \le 14$, $\alpha = 1.26$				
c: $13 \le E_I \le 70$, $\alpha = 1.46$					c: $14 \le E_I \le 42$, $\alpha = 1.26$				
d: $70 \le E_I$, $\alpha = 2.00$					d: $42 \le E_I$, $\alpha = 2.00$				
η	f_a	f_b	f_c	f_d	η	f_a	f_b	f_c	f_d
1.25	0.175	10.4	0.095	0.90	1.25	0.089	0.025	0.040	0.50
1.50	0.480	29.0	0.195	2.15	1.50	0.18	0.083	0.110	1.55
1.75	0.920	39.0	0.295	3.60	1.75	0.29	0.14	0.19	2.80
2.0	1.43	47.0	0.390	5.10	2.0	0.34	0.20	0.27	4.10
2.5	2.55	55.5	0.550	6.80	2.5	0.47	0.30	0.42	6.75
3.0	3.70	60.0	0.680	7.60	3.0	0.56	0.38	0.53	9.00
3.5	4.20	62.5	0.790	8.00	3.5	0.63	0.44	0.61	10.0
4.0	4.30	64.5	0.840	8.15	4.0	0.67	0.50	0.67	11.0
5.0	4.38	65.0	0.850	8.10	5.0	0.73	0.59	0.73	11.5
6.0	4.25	64.0	0.820	7.90	6.0	0.74	0.66	0.74	11.5
7.0	4.10	62.0	0.780	7.50	7.0	0.77	0.70	0.74	11.2
8.0	3.90	59.5	0.750	7.20	8.0	0.78	0.73	0.73	10.8
10.0	3.56	54.0	0.675	6.40	10.0	0.78	0.75	0.69	10.3
15	2.85	43.0	0.530	5.00	15	0.76	0.71	0.60	8.6
20	2.35	35.0	0.440	4.10	20	0.72	0.65	0.51	7.3
25	2.02	29.5	0.375	3.50	25	0.69	0.59	0.44	6.3
30	1.78	26.0	0.325	3.00	30	0.65	0.54	0.39	5.6
40	1.45	20.5	0.262	2.45	40	0.58	0.46	0.32	4.6
50	1.23	17.2	0.215	2.05	50	0.52	0.40	0.275	4.0
60	1.08	15.0	0.186	1.78	60	0.47	0.36	0.240	3.5
80	0.85	11.8	0.146	1.40	80	0.40	0.29	0.195	2.8
100	0.72	9.7	0.120	1.17	100	0.34	0.25	0.165	2.3
					150	0.26	0.185	0.120	1.7
					200	0.22	0.148	0.094	1.3
					300	0.16	0.108		
					400	0.13	0.084		
					500	0.105	0.070		
					600	0.090	0.059		
					800	0.072	0.046		

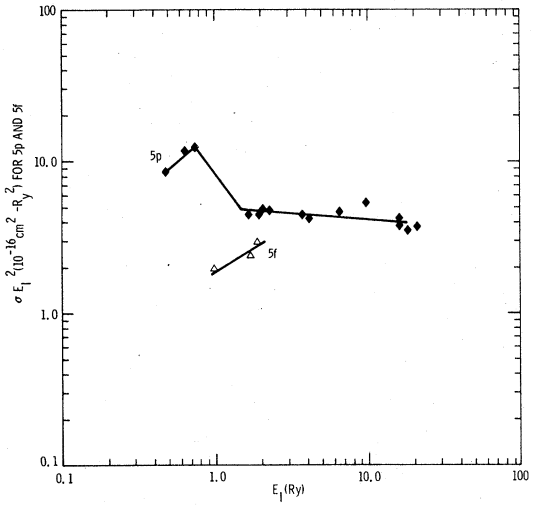

FIG. 5. Calculated $\sigma_{max}(E_I)^2$ for $5p$ and $5f$ subshells.

unless otherwise specified.

In Fig. 7 the electron-ionization cross section for Cs and Cs^+ calculated with the scaled subshell cross sections are compared with experiment. Curve 1 is the Cs(5s) cross section calculated with

TABLE III. Parameters for the scaled $5s$ and $5p$ electron-ionization cross sections; $\sigma_{nl}(\epsilon)(E_I^{nl})^\alpha = f_i(\epsilon/E_I^{nl})$, with f in units of 10^{-16} cm^2 Ry$^\alpha$. The subscripts a–c refer to the following values for α and E_I^{nl}.

$5s$				$5p$			
a: $0.3 \le E_I \le 1.5$, $\alpha = 1.84$				a: $0.46 \le E_I \le 0.75$, $\alpha = 1.17$			
b: $1.5 \le E_I \le 2.5$, $\alpha = 2.74$				b: $0.75 \le E_I \le 1.5$, $\alpha = 3.33$			
c: $2.5 \le E_I \le 30$, $\alpha = 2.00$				c: $1.5 \le E_I \le 20$, $\alpha = 2.08$			
η	f_a	f_b	f_c	η	f_a	f_b	f_c
1.25	0.44	0.70	0.34	1.25	1.90	1.70	0.50
1.50	0.83	1.33	0.65	1.50	3.70	3.30	1.42
1.75	1.14	1.80	0.87	1.75	5.30	5.00	2.40
2.0	1.32	2.12	1.02	2.0	6.40	6.20	3.35
2.5	1.51	2.38	1.20	2.5	8.20	8.00	4.55
3.0	1.61	2.40	1.22	3.0	9.00	8.80	4.90
3.5	1.60	2.25	1.22	3.5	9.50	9.20	5.00
4.0	1.58	2.10	1.18	4.0	9.60	9.30	4.90
5.0	1.40	1.88	1.08	5.0	9.20	9.00	4.65
6.0	1.27	1.68	0.97	6.0	8.50	8.50	4.25
7.0	1.15	1.52	0.90	7.0	7.90	7.90	3.90
8.0	1.03	1.38	0.81	8.0	7.45	7.40	3.55
10.0	0.85	1.15	0.68	10.0	6.60	6.50	3.00
15	0.62	0.80	0.50	15	5.25	4.85	2.18
20	0.47	0.61	0.39	20	4.35	3.90	1.70
25	0.39	0.49	0.33	25	3.75	3.25	1.40
30	0.33	0.41	0.285	30	3.30	2.80	1.18
40	0.25	0.31	0.220	40	2.68	2.20	0.93
50	0.200	0.25	0.180	50	2.26	1.80	0.75
60	0.168	0.21	0.153	60	1.96	1.53	0.64
80	0.125	0.16	0.120	80	1.55	1.18	0.49
100	0.100	0.13	0.098	100	1.30	0.97	0.40

TABLE IV. Parameters for the scaled $5d$ and $5f$ electron-ionization cross sections; $\sigma_{nl}(\epsilon)(E_I^{nl}) = f_i(\epsilon/E_I^{nl})$, with f in units of 10^{-16} cm^2 Ry$^\alpha$. The subscripts a and b refer to the following values for α and E_I^{nl}.

$5d$			$5f$	
a: $0.8 \le E_I \le 4.2$, $\alpha = 1.29$			a: $0.9 \le E_I \le 2.0$, $\alpha = 1.37$	
b: $4.2 \le E_I \le 11.0$, $\alpha = 2.96$				
η	f_a	f_b	η	f_a
1.25	0.48	5.6	1.25	0.135
1.50	0.98	13.2	1.50	0.275
1.75	1.50	21.0	1.75	0.42
2.0	2.00	29.0	2.0	0.57
2.5	2.95	43.0	2.5	0.81
3.0	3.85	56.0	3.0	1.00
3.5	4.52	57.0	3.5	1.15
4.0	5.17	56.0	4.0	1.32
5.0	5.60	53.5	5.0	1.58
6.0	5.60	49.5	6.0	1.80
7.0	5.45	45.5	7.0	2.00
8.0	5.30	43.0	8.0	2.18
10.0	4.80	37.0	10.0	2.28
15	3.92	27.5	15	2.15
20	3.30	22.0	20	1.92
25	2.80	18.3	25	1.75
30	2.50	16.0	30	1.60
40	2.04	12.6	40	1.34
50	1.72	10.4	50	1.15
60	1.50	8.85	60	1.02
80	1.20	6.80	80	0.83
100	1.00	5.60	100	0.70
			150	0.52
			200	0.41
			300	0.29
			400	0.23
			600	0.164
			800	0.129
			1000	0.108

the Herman-Skillman[6] ionization energy, while curve 2 is the $Cs^+(5p)$ cross section. Curve 3 is the sum of 1 and 2 and is in excellent agreement with the measurements of Peart and Dolder[7] for electron ionization of Cs^+. Curve 4 is the calculated Cs(6s) cross section and curve 5 is the sum of the calculated $6s$ and $5p$ cross sections. Curve 5 is lower than the measurements of MacFarland and Kinney.[8] This difference could arise via excitation of autoionizing levels $(5p)^6(6s)+e \rightarrow (5p)^5(6s)(nl) \rightarrow (5p)^6$. To check this a calculated $5p$ total excitation cross section[9] for Xe, with the $(5p)^6 \rightarrow (5p)^5(6s)$ cross section reduced by a factor of 2, scaled by the ratio of $5p$ subshell ionization energy squared was used to approximate the contribution of autoionizing effects to the Cs cross section. Inclusion of the autoionizing contribution

TABLE V. Parameters for the scaled $6s$ and $6p$ electron-ionization cross sections; $\sigma_{nl}(\epsilon)(E_I^{nl})^\alpha = f_i(\epsilon/E_I^{nl})$, with f in units of 10^{-16} cm^2 Ry$^\alpha$. The subscripts a and b refer to the following values for α and E_I^{nl}.

$6s$			$6p$		
a: $0.3 \leq E_I \leq 1.4$, $\alpha = 1.89$			a: $0.34 \leq E_I \leq 0.80$, $\alpha = 1.44$		
b: $1.4 \leq E_I \leq 3.4$, $\alpha = 2.38$			b: $0.80 \leq E_I \leq 2.2$, $\alpha = 2.52$		
	f_a	f_b		f_a	f_b
1.25	0.36	0.62	1.25	1.40	1.30
1.50	0.75	1.10	1.50	3.00	2.35
1.75	1.05	1.45	1.75	4.70	3.50
2.0	1.27	1.70	2.0	6.10	4.60
2.5	1.55	1.98	2.5	8.00	5.80
3.0	1.65	2.04	3.0	8.55	6.50
3.5	1.70	2.04	3.5	8.60	6.80
4.0	1.65	2.00	4.0	8.50	6.90
5.0	1.52	1.86	5.0	8.00	6.70
6.0	1.35	1.70	6.0	7.50	6.40
7.0	1.20	1.52	7.0	7.00	6.00
8.0	1.18	1.40	8.0	6.60	5.60
10.0	0.92	1.18	10.0	5.75	5.00
15	0.66	0.83	15	4.50	3.60
20	0.51	0.66	20	3.70	2.90
25	0.42	0.53	25	3.15	2.40
30	0.36	0.45	30	2.75	2.10
40	0.275	0.35	40	2.20	1.65
50	0.225	0.280	50	1.86	1.36
60	0.185	0.235	60	1.62	1.17
80	0.140	0.178	80	1.28	0.82
100	0.112	0.144	100	1.07	0.75

TABLE VI. Parameters for the scaled $6d$ and $7s$ electron-ionization cross sections; $\sigma_{nl}(\epsilon)(E_I^{nl})^\alpha = f_i(\epsilon/E_I^{nl})$, with f in units of 10^{-16} cm^2 Ry$^\alpha$. The subscripts a and b refer to the following values for α and E_I^{nl}.

$6d$		
a: $0.25 \leq E_I \leq 0.50$, $\alpha = 2.00$		
$7s$		
b: $0.30 \leq E_I \leq 0.40$, $\alpha = 2.00$		
η	f_a	f_b
1.25	0.65	0.44
1.50	1.38	0.80
1.75	2.00	1.05
2.0	2.55	1.22
2.5	3.40	1.40
3.0	3.90	1.42
3.5	4.25	1.38
4.0	4.45	1.32
5.0	4.62	1.20
6.0	4.70	1.08
7.0	4.60	0.98
8.0	4.50	0.90
10.0	4.20	0.74
15	3.50	0.53
20	2.90	0.40
25	2.55	0.32
30	2.27	0.27
40	1.85	0.205
50	1.56	0.163
60	1.36	0.135
80	1.10	0.103
100	0.92	0.084

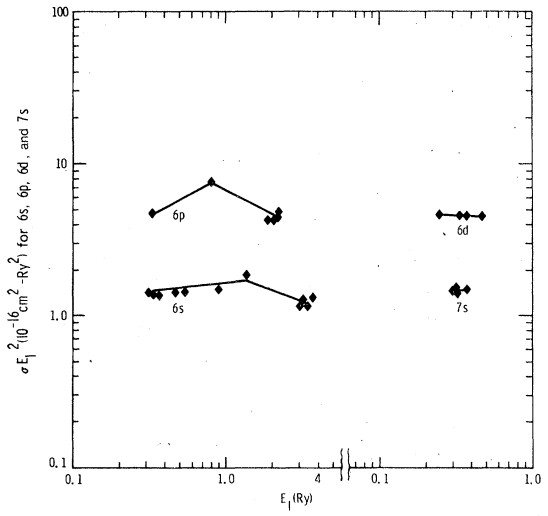

FIG. 6. Calculated $\sigma_{\text{Max}}(E_I)^2$ for $6s$, $6p$, $6d$, and $7s$ subshells.

results in curve 6, which is in excellent agreement with the measurements of MacFarland and Kinney.[8]

In Fig. 8 the electron-ionization cross section for Ba and Ba$^+$ calculated with the scaled subshell cross sections is compared with experiment. Curve 1 is the Ba($5p$) ionization cross section calculated with the Herman-Skillman[6] ionization energy, curve 3 is the sum of the Ba$^+$($6s$) cross sections and the Ba($5p$) cross section, while curve 5 is curve 3 plus autoionization of $(5p)^5(6s)(nl)$ levels calculated by scaling the Xe($5p$) total excitation cross section. Curve 5 is an excellent agreement with the measurements of Peart and Dolder[10] in the 30–200-eV region, but at higher energies the measurements are higher than the calculations (40% at 1000 eV). Curve 2 is the calculated Ba($6s$) ionization cross section, curve 4 is $\sigma(6s)+2\sigma(5p)$ (the factor of 2 arising from the Auger decay subsequent to $5p$ subshell ionization), while curve 6 is curve 4 plus autoionization of $(5p)^5(6s)^2(nl)$ levels calculated by scaling the Xe($5p$) total excitation cross section. Between 15 and 100 eV, curve 6 is in excellent agreement with the measurements of Okuno.[11] Above 100 eV the measure-

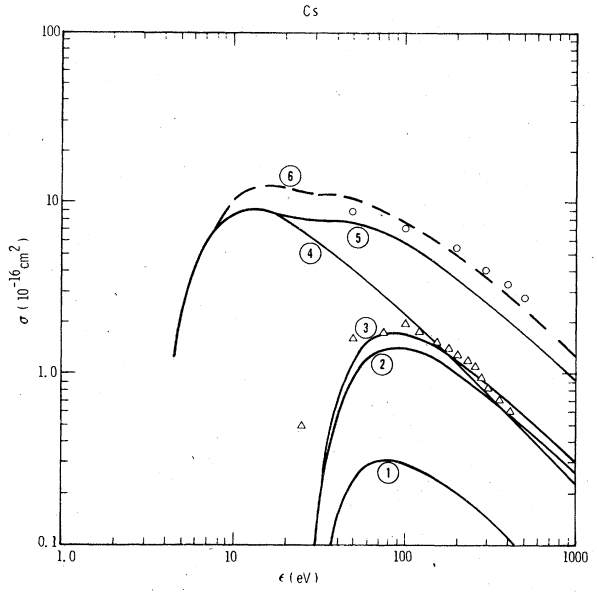

FIG. 7. Calculated and experimental electron-ionization cross section of Cs and Cs^+. Curve 1 is the calculated $5s$ cross section for Cs; curve 2 is the calculated $Cs^+(5p)$ cross section; and curve 3 is their sum. The measurements on Cs^+ (triangles) are from Ref. 7. Curve 4 is the Cs($6s$) cross section; curve 5 is the sum of the $6s$ and $5p$ cross sections, while curve 6 is curve 5 plus the contribution of autoionization following $5p$ excitation. The experimental points (circles) are from Ref. 8.

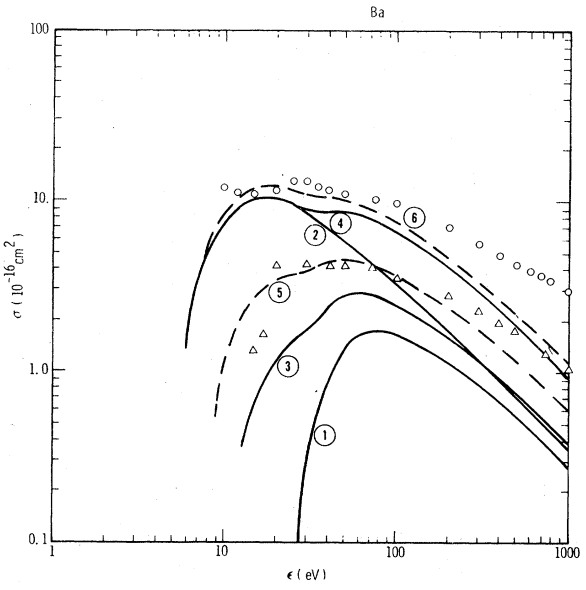

FIG. 8. Calculated and experimental electron-ionization cross section of Ba and Ba^+. Curve 1 is the Ba($5p$) cross section; curve 3 is the sum of the Ba($5p$) and $Ba^+(6s)$ cross sections; and curve 5 is curve 3 plus the contribution of autoionization. The experimental data (triangles) are from Ref. 10. Curve 2 is the Ba ($6s$) cross section; curve 4 is $\sigma(6s)+2\sigma(5p)$, while curve 6 is curve 4 plus the contribution of autoionization. The experimental data (circles) are from Ref. 11.

ments are significantly higher than the calculations. This is similar to the discrepancy at high energy between the calculations and Okuno's measurements on Ca and Sr (Fig. 11 of Ref. 2). At 500 eV Okuno's measured cross section is a factor of 2 higher than the calculations. But at 500 eV Okudaira[12] measures a ratio of doubly to singly charged ions ($\sigma_{5p}/\sigma_{6s}+\sigma_{\text{auto}}$ [where σ_{auto} is σ(autoionization)]) of 0.79. The calculated value is 0.66. If one assumes that Okudaira's factor is correct, and the calculated σ_{6s} and σ_{auto} are correct the cross section at 500 eV is 2.58×10^{-16} cm², a factor of 1.2 higher than the calculation, but substantially less than Okuno's measured value.

In Fig. 9 the calculated σ_{6s} and $\sigma_{6s}+\sigma_{5d}$ for Au are shown along with the measurements of Schroeer *et al.*[13] Moore's tables[5] indicate that the terms of the $(5d)^9(6s)^2$, $(5d)^9(6s)(6p)$, and $(5d)^9(6s)(7s)$ configurations are bound. Since transitions to these configurations dominate the $5d$ subshell total excitation cross section, autoionization effects on the electron-ionization cross section are negligible. Further the $(5d)^9(6s)\ ^1D$ and ^3D levels in Au^+ are bound, so there is no Auger decay following $5d$ ionization. Thus $\sigma_{6s}+\sigma_{5d}$ is the total

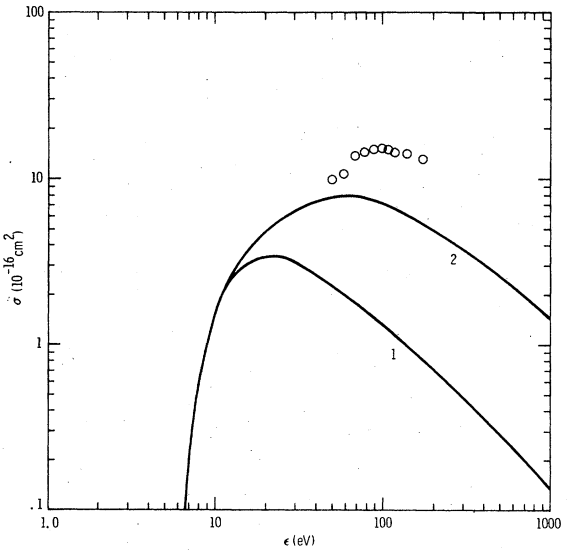

FIG. 9. Calculated and experimental electron-ionization cross section of Au. Curve 1 is the $6s$ cross section and curve 2 is the sum of $6s$ and $5d$ cross sections. The experimental data (circles) are from Ref. 13.

electron-ionization cross section of Au. Schroeer *et al.*[13] have also measured the electron-ionization cross section of Cu with the same apparatus. Their results are a factor of 1.85 larger than those of Crawford.[14] Crawford's measurements are in reasonable agreement with my calculations in Zn. The peak cross section measured by Schroeer *et al.*[13] for Au (15.37×10^{-16} cm^2 at 100 eV) is a factor of 1.92 larger than the calculated peak cross section (at 70 eV). This suggests a calibration error of 1.85 in the measurements of Schroeer *et al.*

In Fig. 10 the calculations on Hg are shown and compared with the measurements of Jones,[15] Liska,[16] Smith,[17] and Harrison.[18] For Hg the calculations were obtained both by scaling and by direct calculation. The experimental $5d$ ionization threshold in Hg is 15.5 eV, the value used in the direct calculation was 15.8 eV. However, the experimental $6s$ ionization threshold is 10.43 eV, while the value used in the calculation was 7.76 eV. In Fig. 10 the calculated σ_{6s}, $\sigma_{6s}+\sigma_{5d}$, and $\sigma_{6s}+\sigma_{5d}+\sigma_{\text{auto}}$ are shown. The solid curves were obtained from the scaled cross sections using experimental ionization energies, the dashed curves are the direct calculations. The difference between the two calculated total cross sections is due almost entirely to the choice of $6s$ ionization threshold. Moore's tables[5] indicate that the $(5d)^9(6s)^2\,^2D$ term in Hg^+ is bound, so ionization of the $5d$ subshell is not followed by Auger decay. However, Moore's tables[5] indicate that all configurations of the form $(5d)^9(6s)^2(nl)$ will autoionize and the cross section for $5d$ excitation followed by autoionization is included in Fig. 10. The calculations are in excellent agreement with the experimental measurements though the calculated cross section is lower at high energy (by 25% at 1 keV). The neglected inner-shell cross sections (0.16×10^{-16} at 1 keV) can account for most of the discrepancy, but to evaluate the neglected cross sections properly *vis a vis* the measurements requires one trace through the subsequent Auger cascade to determine the mean ion charge resulting from the specific inner-shell ionization. This has not been done.

There are experimental measurements on the electron ionization cross section of both Tl and Tl^+. To calculate a total cross section that can be compared with the measurements is a formidable task for two reasons. For a $5d$ vacancy to Auger decay requires that the $5d$ ionization energy be greater than the sum of the first two ionization potentials. From Moore's tables[5] this is 26.53 eV in Tl. The $5d$ ionization energy in the tables of Herman and Skillman[6] is 24.0 eV, while Mann's Hartree-Fock calculations[19] give 26.34 eV. Further there is term splitting of the $(5d)^9(6s)^2(6p)^1$ configuration. Thus it is likely that some but not all of the terms will Auger decay. In the calculation Auger decay is neglected. The second difficulty is that some of the terms of the $(6s)^1(6p)^2$ configuration can autoionize. The excitation cross section for the resonance transition $(6s)^2(6p)-(6s)(6p)^2$ is expected to be large. However, for the autoionizing terms one expects configuration interaction to mix bound and autoionizing levels in such a way that, effectively, excitation cross section is transferred from the autoionizing to the bound levels. In addition, of the terms of the $(6s)^1(6p)^2$ configuration that have a substantial ex-

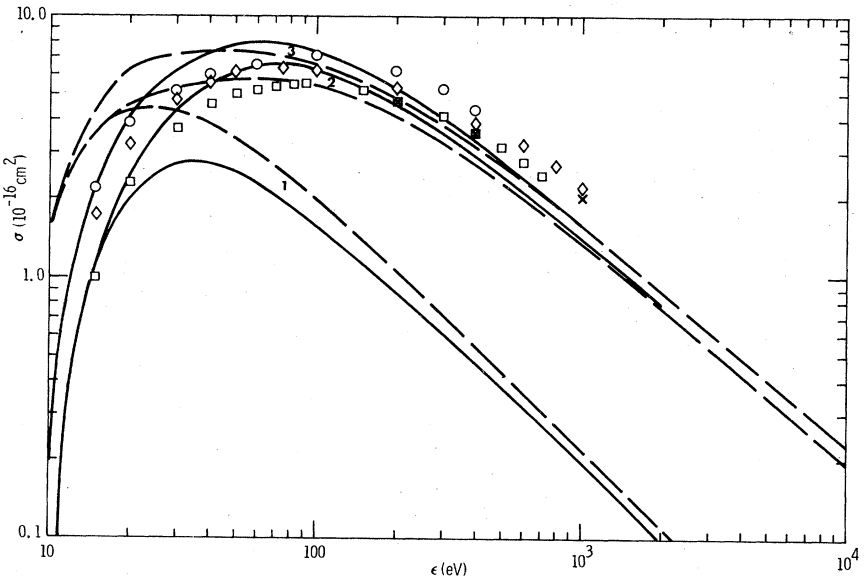

FIG. 10. Calculated and experimental electron-ionization cross section of Hg. Curves 1 are the $6s$ cross sections; curves 2 are the sum of $(6s)$ and $5d$ cross sections, while curves 3 are curves 2 plus autoionization. The solid curves used experimental ionization energies, while the dashed curves use calculated ionization energies. The measurements (circles, exxes, squares, and diamonds) are from Ref. 15–18, respectively.

citation cross section from $(6s)^2(6p)^1$, (i.e., ^2D, ^2P, and ^2S), parity considerations forbid Auger decay of the ^2P term. Thus we assume this term does not add an autoionization contribution to the measured electron-ionization contribution. Then for Tl the contribution of autoionization due to $6s$ excitation to the measured electron-ionization cross section is estimated to be

$$\tfrac{2}{3}\tfrac{5}{6}[E_{6s}(\mathrm{Tl})/E_{6s}(\mathrm{Hg})]^2\sigma_{\mathrm{exc.}}^{\mathrm{tot}}(\mathrm{Hg})$$

(exc. stands for excitation).

In Fig. 11 the calculated electron-ionization cross sections are shown for Tl and Tl^+ along with the measurements of Divine *et al.*[20] on Tl^+ and McFarland[21] and Shimon *et al.*[22] on Tl. Curve 1 is the $Tl^+(6s)$ ionization cross section while curve 2 is the sum of the $Tl^+(5d)$ and $(6s)$ cross sections. The $Tl^+(5d)$ ionization energy used was 2.37 Ry, the mean of the Herman-Skillman[6] $Tl(5d)$ ionization energy and the $Tl^{2+}(5d)$ ionization energy obtained from Moore's tables.[5] The $Tl^+(5d)$ electron excitation cross section is dominated by $(5d)^{10}(6s)^2-(5d)^9(6s)^2(6p)$ transitions, and many of the terms of $(5d)^9(6s)^2(6p)$ are listed as bound levels in Moore's tables.[5] Thus excitation followed by autoionization should make a negligible contribution to the measured electron-ionization cross section in Tl^+. Furthermore, since Auger decay of a $5d$ hole in Tl is a marginal process, it is unlikely to occur in Tl^+. Consequently curve 2 is the calculated electron-ionization cross section of Tl^+. The calculated Tl^+ cross section is somewhat higher than the measured value of Divine *et al.*[20] (20% at 1 keV). Curve 3 is the $Tl(6p)$ ionization cross section, curve 4 is the sum of σ_{6p} and σ_{6s}, while curve 5 is the sum of $\sigma_{6p}+\sigma_{6s}+\sigma_{5d}$. Curve 6 is the sum of the three subshell cross sections plus the approximate contribution due to autoionization. Curve 6 is higher than the measurements of McFarland[21] and Shimon *et al.*[22] at low energy, and lower than their measurements at high energies. Because of the approximations made in the calculation, it cannot be used to distinguish between the two sets of measurements.

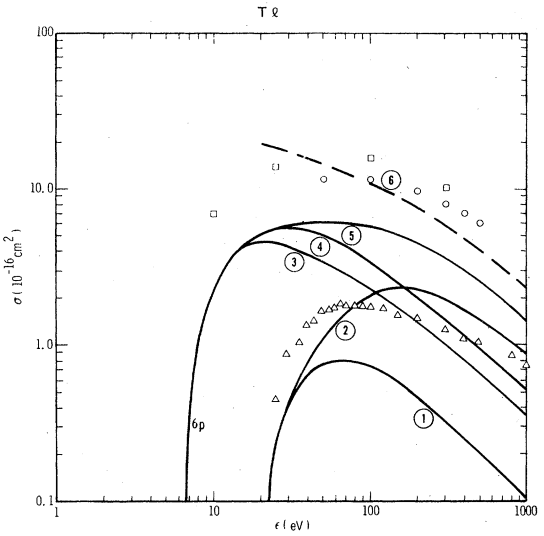

FIG. 11. Calculated and experimental electron-ionization cross section of Tl and Tl^+. Curve 1 is the $Tl^+(6s)$ cross section, and curve 2 is the sum of $Tl^+(6s)$ and $(5d)$ cross sections. The measurements (triangles) are from Ref. 20. Curve 3 is the Tl $(6p)$ cross section; curve 4 is the sum of $Tl(6p)$ and $(6s)$ cross sections; curve 5 is the sum of $(6p)$, $(6s)$, and $(5d)$ cross sections, while curve is curve 5 plus autoionization. The measurements (circles and squares) are from Refs. 21 and 22, respectively.

In Fig. 12 the calculated electron-ionization cross section of Pb is shown, along with the measurements of Pavlov *et al.*[23] Curves 1, 2, and 3 are $\sigma(6p)$, $\sigma(6p)+\sigma(6s)$, and $\sigma(6p)+\sigma(6s)+2\sigma(5d)$, respectively. The calculation includes Auger decay but neglects autoionization following $(6s)^2(6p)^2-(6s)(6p)^3$ excitation. From Moore's tables[5] the $Pb(6p)$ ionization energy is 7.42 eV and the $6s$ is 16.7. A crude estimate would locate the $(6s)(6p)^3$ configuration 1.9 eV above the ionization threshold. However, term splitting, as well as configuration and spin-orbit interaction will shift some terms below the ionization threshold. Moore's tables[5] list no terms of $(6s)^1(6p)^3$, either above or below the ionization threshold. With the neglect of a possible autoionization contribution, the calculated cross section (curve 3) is in excellent agreement with the measurements of Pavlov *et al.*[23] This agreement shows the power of the scaling technique. Since $Z=82$ for Pb, it was one of the elements for which direct calculations were done. However, the Herman-Skillman[5] $6s$ and $6p$ ioni-

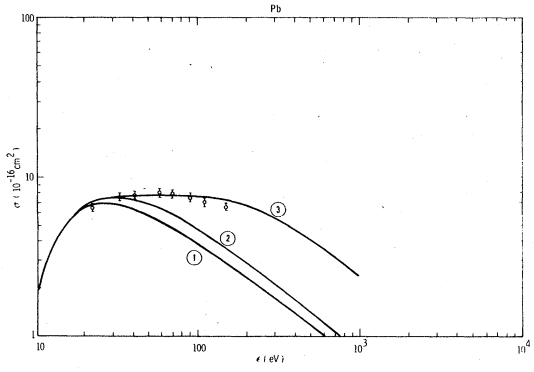

FIG. 12. Calculated and experimental electron-ionization cross section of Pb. Curve 1 is $\sigma(6p)$; curve 2 is $\sigma(6p)+\sigma(6s)$; and curve 3 is $\sigma(6p)+\sigma(6s)+2\sigma(5d)$. The measurements are from Ref. 23.

zation energies, 12.1 and 5.77 eV, respectively, are significantly lower than the measured values, 16.7 and 7.42 eV, respectively. The direct calculation resulted in a cross section almost a factor of two larger than the measured values.

IV. ELECTRON IONIZATION OF THE NOBLE-GAS METASTABLE LEVEL

Ton-That and Flannery[4] have pointed out that electron ionization of the noble-gas metastable level $(np)^5[(n+1)s]^3P_2$ plays an important role in modeling noble-gas eximer lasers. They report cross section calculations using both the Born approximation and the binary encounter approximation. These cross sections can be calculated using the scaled cross sections herein and in Ref. 2. The calculations are shown in Figs. 13(a)–13(d). Curve 1 is outer s electron-ionization cross section, while curve 2 is the sum of $(n+1)s$ and np ionization cross sections. The open circles and triangles are the calculations Ton-That and Flannery,[4] in the half-range Born approximation for the outer s electron and in the binary encounter approximation for the total cross section. The solid circles are the measurements of Dixon *et al.*[24] for Ne and Ar. For Ne and Ar the half-range Born approximation calculations of Ton-That and Flannery are in excellent agreement with my calculated outer s electron cross section. My total cross section is in excellent agreement with the measurements. For Ne and Ar, the binary encounter total cross section is higher than both the measurements and my calculations. For Kr and Xe the half-range calculations of Ton-That and Flannery are higher than my calculations at 10 eV, but in reasonable agreement at high energy. At high energy and binary encounter total cross section is higher than my Kr calculation but in reasonable agreement with my Xe calculation.

For electron ionization from metastable excited states of the noble gases, the scaled cross sections are in excellent agreement with the measurements of Dixon *et al.*,[24] and the half-range Born

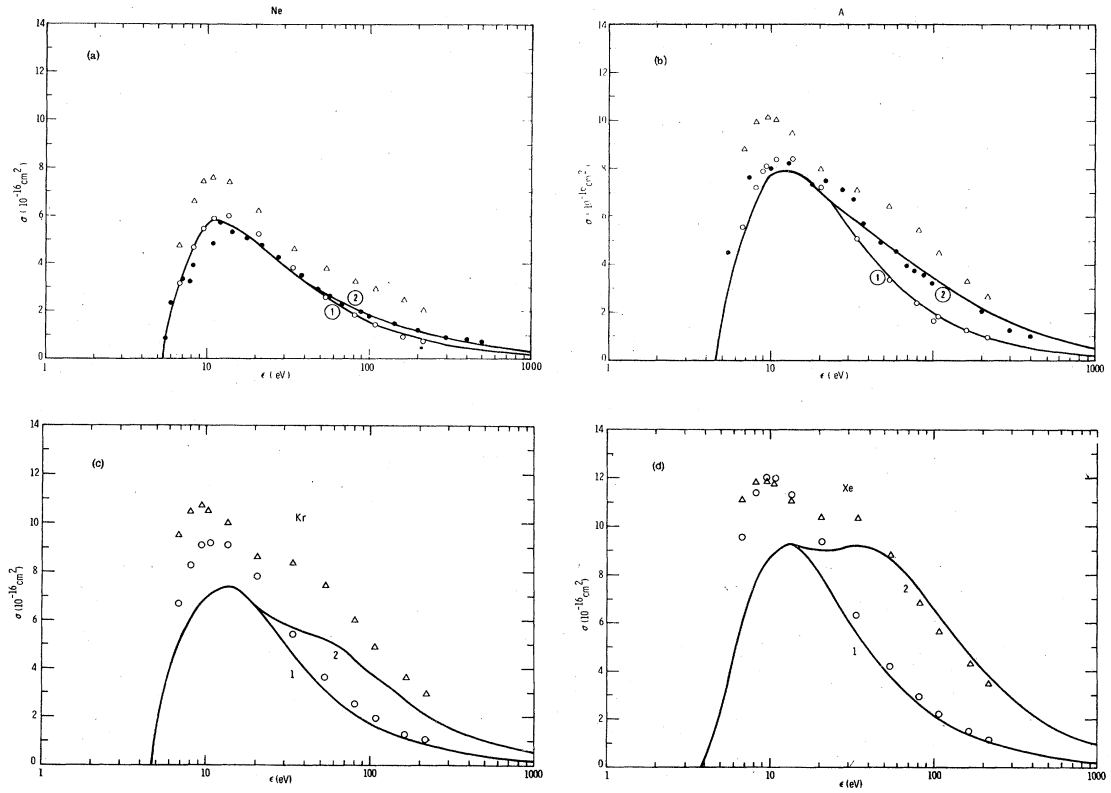

FIG. 13. (a)–(d) Calculated and measured electron ionization cross sections for the noble-gas metastable level $(np)^5[(n+1)s]^3P_2$. Curve 1 is $\sigma((n+1)s)$ and curve 2 is $\sigma((n+1)s)+\sigma((np)^5)$. The open circles (triangles) are the half-range Born approximation (binary encounter) calculations of Ref. 4 for $\sigma((n+1)s)$ $[\sigma((n+1)s)+\sigma((np)^5)]$. The solid circles are measurements from Ref. 24.

calculations of Ton-That and Flannery,[4] further illustrating the utility of the scaled cross sections.

V. SEQUENTIAL IONIZATION OF Ni AND Au

The scaled cross sections were used to calculate the cross sections for Ni^{+1}–Ni^{+14} and Au^{+3}–Au^{+14}, using Herman-Skillman[6] ionization energies for the ions. For Ni the $3d$, $3p$, $3s$, and $2p$ subshells were included; for Au the $5d$, $5p$, $5s$, $4f$, and $4d$ subshells were included. In addition, cross sections were calculated with the formula of Lotz[1] for the same subshells and ionization energies. In Fig. 14 the results are compared for Ni. At high energy the agreement is excellent. For higher states of ionization the Lotz cross section is more strongly peaked at low energy. In Fig. 15 a similar comparison is made for Au. Here there is no agreement at any energy between the two sets of calculations. In Fig. 16 the peak cross section for each of the subshells is plotted as a function of the charge stage of the Au ion. For the $5p$ subshell the two sets of calculations are in excellent agreement. For the $5s$ subshell the agreement is reasonable. For the $4f$ and $4d$ subshells the scaled cross sections are a factor of three larger than Lotz's values. For the $5d$ subshell the scaled cross sections are larger than Lotz's for low-ionization states, and in reasonable agreement high-ionization states.

Since Lotz's expression is semiempirical, and there are no measurements available on $4f$ subshell ionization, and only indirect measurements

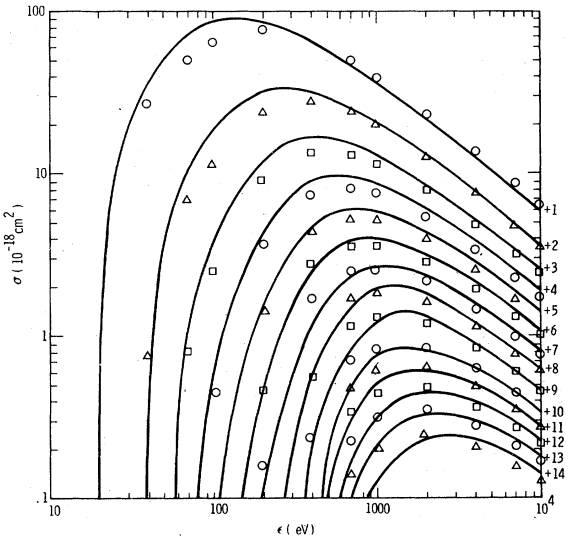

FIG. 14. Calculated electron-ionization cross sections of Ni^{+1}–Ni^{+14}. The solid curves are obtained from the scaled cross sections. The circles, triangles, and squares are from the expression in Ref. 1.

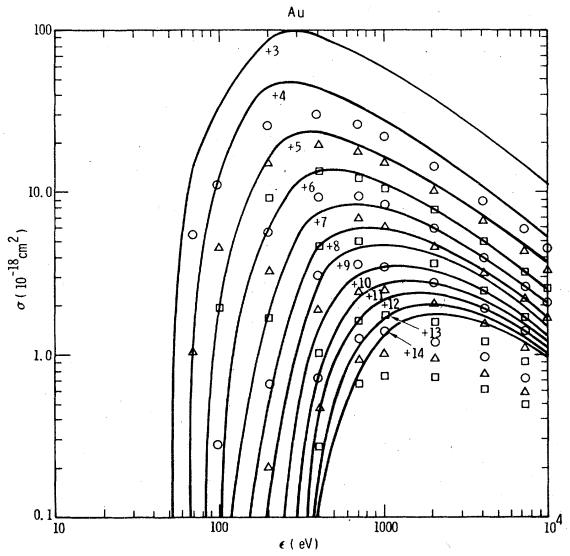

FIG. 15. Calculated electron-ionization cross sections of Au^{+3}–Au^{+14}. The solid curves are obtained from the scaled cross sections. The circles, triangles, and squares are from the expression in Ref. 1.

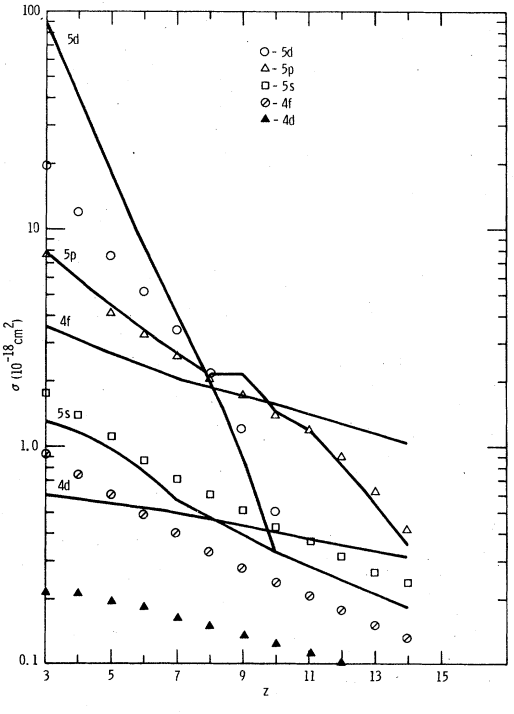

FIG. 16. Calculated Au peak subshell electron-ionization cross section versus state of ionization. The solid curves are obtained from the scaled cross sections, while the points are from the expression in Ref. 1.

on $4d$ and $5d$ subshell ionization it is not surprising that Lotz's parametrization for these subshells lead to results significantly different from the scaled results. On the other hand, measurements on Xe were available, and presumably, incorporated in Lotz's formula. This accounts for the excellent agreement in the $5p$ cross section.

VI. CONCLUSIONS

Here and in Ref. 3 scaled electron-ionization cross sections have been presented for all occupied subshells in atoms with $Z \leq 102$. For those high-Z elements for which data is available there is good agreement between the calculated cross sections obtained from the scaling procedure and the measurements. The scaling procedure was extrapolated to calculate electron-ionization cross sections for the metastable states of the noble gases, and led to excellent agreement with measurements in Ne and A. The scaling procedure was used to calculate cross sections for sequential ionization of Ni and Au. For Ni ions the resulting cross sections were in good agreement with Lotz's semiempirical cross section, but for Au ions there was a substantial disagreement. By examining the subshell cross sections for Au ions, it was found that the disagreement arose from subshells for which there was no or little experimental data with which to construct a semiempirical cross section.

These calculations on electron ionization in high-Z elements have shown the utility of the scaling hypothesis. The extension of the scaling hypothesis to proton ionization, proton and electron stopping power, and secondary-electron distributions will be discussed in later papers.

[1]W. Lotz, Z. Phys. 232, 101 (1970).
[2]E. J. McGuire, Phys. Rev. A 16, 62 (1977).
[3]E. J. McGuire, Phys. Rev. A 16, 73 (1977).
[4]D. Ton-That and M. R. Flannery, Phys. Rev. A 15, 517 (1977).
[5]C. E. Moore, *Atomic Energy Levels*, Natl. Bur. Stds. (U.S.) Circ. No. 467 (U.S. GPO, Washington, D.C., 1957), Vol. III.
[6]F. Herman and S. Skillman, *Atomic Structure Calculations* (Prentice-Hall, Englewood Cliffs, N.J., 1963).
[7]B. Peart and K. Dolder, J. Phys. B 8, 56 (1975).
[8]R. H. McFarland and J. D. Kinney, Phys. Rev. 137, A1058 (1965).
[9]A systematic study of electron-excitation cross sections will be published in the future.
[10]B. Peart and K. T. Dolder, J. Phys. B 2, 872 (1968).
[11]Y. Okuno, J. Phys. Soc. Jpn. 31, 1189 (1971).
[12]S. Okudaira, J. Phys. Soc. Jpn. 29, 409 (1970).
[13]J. M. Schroeer, D. H. Gündüz, and S. Livingston, J. Chem. Phys. 58, 5135 (1973).
[14]C. K. Crawford, Technical Report No. 1 (Particle Optics Laboratory, MIT, Cambridge, Mass., 1969) (unpublished).
[15]T. J. Jones, Phys. Rev. 29, 822 (1927).
[16]J. W. Liska, Phys. Rev. 46, 169 (1934).
[17]P. J. Smith, Phys. Rev. 37, 808 (1931).
[18]H. Harrison, Ph.D. thesis (Catholic University of America, Washington, D.C., 1956) (unpublished).
[19]J. B. Mann, Los Alamos Scientific Laboratory Report No. LASL-3690, 1967 (unpublished).
[20]T. F. Divine, R. K. Feeney, W. E. Sayle, II, and J. W. Hooper, Phys. Rev. A 13, 54 (1976).
[21]R. H. McFarland, Phys. Rev. 159, 20 (1967).
[22]L. L. Shimon, E. I. Nepiipov, and I. P. Zapesochnyi, Zh. Tekh. Fiz. 45, 688 (1975) [Sov. Phys. Tech. Phys. 20, 434 (1975)].
[23]S. I. Pavlov, V. I. Rakhovskii, and G. M. Fedorova, Zh. Eksp. Teor. Fiz. 52, 21 (1967) [Sov. Phys. JETP 25, 12 (1967)].
[24]A. J. Dixon, M. F. A. Harrison, and A. C. H. Smith, *Abstracts of Papers of Eighth International Conference on the Physics of Electronic and Atomic Collisions*, edited by B. C. Cobic and M. V. Kurepa (Institute of Physics, Belgrade, Yugoslavia, 1973), Vol. 1, p. 405.